Effective medium approximations for modeling optical reflectance from gratings with rough edges

Brent C. Bergner,[1,2] Thomas A. Germer,[1] and Thomas J. Suleski[2]

[1]*National Institute of Standards and Technology, Gaithersburg, MD 20899*

[2]*Department of Physics and Optical Science, University of North Carolina at Charlotte, Charlotte, NC 28223*

ABSTRACT

Line edge roughness (LER) has been identified as a potential source of uncertainty in optical scatterometry measurements. Characterizing the effect of LER on optical scatterometry signals is required to assess the uncertainty of the measurement. However, rigorous approaches to modeling the structures that are needed to simulate LER can be computationally expensive. In this work, we compare the effect of LER on angle resolved scatterometry signals computed using an effective medium approximation to those computed with realizations of rough interfaces. We find that for correlation lengths much less than the wavelength but greater than the rms roughness, that an anisotropic effective medium approximation provides a satisfactory approximation in the cases studied.

OCIS Codes: 050.1960, 240.1770

1. INTRODUCTION

The optical reflectance of a periodic structure can depend strongly on the profile of that structure. By measuring the dependence of the reflectance on polarization and either angle of incidence or wavelength, with prior knowledge of the space of possible structures, and solving the inverse scattering problem, the profile can be determined. Typically, the inverse problem is solved by parameterizing the structure, solving the forward scattering problem, and searching, via a library search or regression analysis, for a best match between the measurement and the forward scattering solution. The method, coined *scatterometry*, is remarkably sensitive, even when the structure features are much smaller than the wavelength of the light, often with precisions in the subnanometer regime [1]. For that reason, the semiconductor industry has embraced scatterometry as a method for monitoring and controlling process [2,3]. Scatterometry, however, requires significant *a priori* knowledge of the periodic structure, usually a grating, and is subject, like any measurement technique, to numerous sources of error.

Line edge roughness (LER) has been identified as a potentially significant source of uncertainty for these measurements [4]. While the models used in the forward scattering problem are typically two-dimensional in nature and one-dimensionally periodic, roughness imposes a three-dimensional nature with no periodicity to the problem. As a result, most approaches towards solving Maxwell's equations in the presence of roughness become significantly more difficult to implement. Approximate methods, if found to be accurate, are desired. In previous work, line variations were treated by maintaining the two-dimensional nature of the grating, increasing the period to include multiple lines, and randomly varying each line's profile [5]. The resulting simulations agreed very

well with a model in which the reflected field was approximated by an average over the field from an appropriate distribution of gratings. However, the two-dimensional nature of these simulations limits the validity of the results to long range variations along the lines. Other studies have investigated LER both experimentally and theoretically but have limited them to square wave modulations of the lines [6-8].

In this article, we investigate the effects of short range roughness along the edge of the grating. We begin by approximating the rough grating as a two dimensionally periodic structure with random variations along the lines. We perform simulations using an implementation of rigorous coupled-wave (RCW) theory appropriate for two-dimensionally periodic gratings [9] and average the results over realizations of an ensemble of line edge profiles. Since these computations are extremely time-consuming, we attempt to approximate the roughness using effective medium boundary layers. This approximation simplifies the problem to one which can be solved using a RCW solution for a one-dimensionally periodic grating [10-13].

In Section 2, we briefly outline the RCW theories we used for the one- and two-dimensionally periodic structures. In Section 3, we describe how we generate self-affine line edge profiles and show that these structures yield results that differ from simple rectangular or sinusoidal line edge profiles. In section 4 we describe the effective medium approximation (EMA) that we used to approximate the LER. In Section 5, we present the comparison between the models.

2. RCW SIMULATIONS

RCW theories supply approximate solutions to Maxwell's equations for periodic, layered media, which converge to exact solutions provided sufficient field orders are maintained. Complete

descriptions of the RCW theories are beyond the scope of this paper and are best left to the original references [9-13]. In this section, we describe the key elements needed to replicate the simulations. For one-dimensionally periodic gratings, including those with EMA boundaries, we implemented the theory described by Moharam *et al.* [10,11] with a modification proposed by Li [12] and Lelanne and Morris [13]. The theory was further extended to allow for anisotropic media in the grating [14]. In this study, we limited our scope to binary gratings (those with vertical sidewalls). We thus divided the space into a region above the grating, the grating region itself, and a region below the grating. The fields in each of the three regions were expanded in a truncated Floquet series, maintaining 21 orders from −10 to +10. The 1DRCW theory requires Fourier series expansions coefficients for $\varepsilon_y(x)$, $\varepsilon_z(x)$ and $1/\varepsilon_x(x)$ where $\varepsilon_i(x)$ is the dielectric permittivity for the fields in the ith direction and x is along the grating vector, y is along the lines, and z is out of the sample plane (see Fig. 1).

For two-dimensionally periodic gratings, with random line edge functions, we implemented the theory described by Li [9] (2DRCW). Structures were defined on a 2048×2048 grid, upon which the required Fourier series expansions of the dielectric permittivity were performed. The fields in each of the three regions were expanded in a truncated Floquet series, maintaining 861 orders from −10 to +10 in the grating direction (x) and from –20 to +20 in the transverse direction (y). We chose the same number of orders (21) in the grating direction as we used for the 1DRCW theory, so that the results were identical for a nominal grating evaluated by either theory. We performed a small subset of the simulations using ±30 orders in the transverse direction and found that those results were well within 0.005 of those obtained using ±20 orders. The dimensions of the rectangular unit cell were the nominal grating period in the x direction and 200 nm in the y direction (along the line).

Because of the additional transverse field orders required for 2DRCW simulations, and because the calculations are dominated by matrix multiplications and inversions, the computational time was approximately $861^3/21^3$ = 68921 times slower than the 1DRCW simulations. The computer code for 1DRCW is provided online [15], while that for 2DRCW is forthcoming.

We applied roughness to a number of nominal binary gratings. Except where noted, the results that we present are limited to a P_x = 200 nm pitch binary grating consisting of w = 100 nm wide, h = 200 nm high silicon lines on a silicon substrate (see Fig. 1). We calculated the angular dependence of the specular, zero-order reflectance for s-polarization (transverse electric, TE, with electric field along the y direction) and p-polarization (transverse magnetic, TM, with magnetic field along the y direction) at a wavelength of 633 nm. The grating vector was aligned with the plane of incidence (often referred to as classical mounting). Silicon gratings were chosen because the effects of LER were found to be much stronger when there is a large index contrast between the grating and the surrounding medium. For example, we found that the root mean square change in the reflectance due to LER is an order of magnitude larger for a silicon grating than for a similar photoresist grating on a silicon substrate. Figure 2 shows the specular reflectance for both polarizations from the nominal grating, calculated by 1DRCW.

3. GENERATION OF ROUGHNESS PROFILES

We simulated reflection from gratings having a variety of line edge profiles. While some authors have suggested more complex models of LER [16], others have suggested that self-affine functions provide adequate descriptors for real line edge profiles [17]. A self-affine function has an autocorrelation function $A(\rho)$ of the form:

$$A(\rho) = \exp[-(\rho/\xi)^{2\alpha}] \quad (1)$$

where ρ is the distance between two points along the nominal edge, ξ is the linear correlation length of the rough edge, and α is a roughness exponent. The roughness exponent, also referred to as the Hurst exponent, is related to the fractal dimension of the edge and can be used to describe the relative amount of high frequency content in the power spectrum. Profiles with Gaussian autocorrelation functions have $\alpha = 1$, and profiles with exponential autocorrelation functions have relatively more high frequency content and $\alpha = 1/2$. Various process steps used to lithographically fabricate gratings are thought to create edge profiles with different correlation length and roughness exponents, and some processes, such as reactive ion etching, may introduce some directionality to the roughness [18]. In this paper we examine the effect of a rough edge (modulations along the *y* direction) on the scattering from a sub-wavelength silicon grating. Calculating the reflectance from gratings that exhibit variations in the sidewall (modulations along both the *y* and *z* directions) would not have been practical, and insight can be gained into the application of the approximation methods using the two-dimensionally periodic LER models.

An examination of the literature on LER [16,18-22] indicates that typical values for the correlation length range between 5 nm and 30 nm, roughness exponents range between 0.15 and 1, and typical rms roughness values are around 2.5 nm. For the simulations presented here, we will examine a grating with LER characterized by σ = 2.5 nm, ξ = 20 nm, and α = 0.5.

Random profiles are numerically generated by calculating the power spectral density $P(k)$ function from the Fourier transform of $A(\rho)$ (Wiener-Khinchin theorem):

$$P(k) = \int A(\rho) \exp(ik\rho) d\rho$$

The square root of $P(k)$ is proportional to the absolute value of the Fourier transform of the random function we are seeking. To randomize the function, we apply a random phase to each frequency component. Thus, the edge profile function $\Delta x(y)$ can be found from the inverse Fourier transform of the result,

$$\Delta x(y) = a\int [P(k)]^{1/2} \exp[i\phi(k) - iky]dk$$

where $\phi(k) = \phi^*(-k)$ is a random phase uniform on the range $[0, 2\pi)$. The constant a was chosen to ensure a specific root-mean-square roughness σ. Separate functions are created for each of the two edges of the line. Figure 3 shows four examples of line edge profiles with different correlation lengths and roughness exponents.

Because the edge profile functions are random, it is necessary for us to average the optical simulation results over a number of realizations of the ensemble. We found that 15 realizations were sufficient to obtain reasonable convergence of the mean. The inclusion of ensemble averaging is an additional, but necessary, computational burden to performing these simulations. To test the necessity of performing the simulations with random edge profiles, rather than square wave or sinusoidal edge profiles, we performed a comparison of the optical responses from square wave and sinusoidal edge profiles (with rms amplitudes of 2.5 nm and periods P_y = 20 nm) with the ensemble average of random profiles ($\xi = 20$ nm, $\alpha = 1/2$, $\sigma = 2.5$ nm). The square wave and sinusoidal variations were correlated between the two edges of the line. Figure 4 shows the results from that comparison, expressed as a change in reflectance $R^{\text{rough}} - R^{\text{nom}}$, where R^{rough} is the reflectance calculated for the rough line and R^{nom} is that calculated for the nominal line. The results for the random modulations clearly differ from those of the sinusoidal and square wave modulations. For that reason, and because natural roughness is typically not periodic, we choose to focus our attention

in the remaining paper on the self-affine randomly modulated edge functions. Note that for the RCW simulations even these randomly modulated edge functions are repeated on a periodic basis. However, we have attempted to minimize the effects of this periodicity by using a period along the length of the line that is as large as possible without excessively increasing the number of transverse orders needed for the solution to converge.

4. EFFECTIVE MEDIUM APPROXIMATION

The optical properties of composite materials can often be approximated by a uniform effective medium when the length scales associated with the local variations in permittivity are small compared to the wavelength of the light in the media. In ellipsometric measurements of thin film stacks, the reflection and transmission coefficients of a rough surface are often calculated by replacing the rough interface by a thin film having a thickness related to the amplitude of the roughness and a permittivity derived from an appropriate effective medium approximation (EMA) [23-25]. In a similar manner, as illustrated in Fig. 1, this paper compares the 2DRCW simulations performed using random edge profiles with a much simpler EMA-based model that can be evaluated using 1DRCW.

We will use a generalized anisotropic Bruggeman EMA to model the effective medium layers. This model can be derived from the generalized form of Maxwell Garnett's effective medium approximation [26] using the expression for the polarizability of ellipsoidal particles [27],

$$\frac{\varepsilon_{\mathrm{eff}} - \varepsilon_0}{\varepsilon_0 + L(\varepsilon_{\mathrm{eff}} - \varepsilon_0)} = \sum_{i=1}^{M} f_i \frac{\varepsilon_i - \varepsilon_0}{\varepsilon_0 + L(\varepsilon_i - \varepsilon_0)} \tag{1}$$

where $\varepsilon_{\mathrm{eff}}$ is the effective medium permittivity, ε_0 is the permittivity of the host medium, and ε_i and f_i are the permittivities and volume fractions of each of the M materials. The depolarization

factor L depends upon the shape of the ellipsoids and the direction of the electric field: for spheres, $L_x = L_y = L_z = 1/3$, for highly prolate ellipsoids (needles) aligned along the z direction, $L_x = L_y = 1/2$ and $L_z = 0$, and for highly oblate ellipsoids (plates) aligned along the y direction $L_x = L_z = 0$ and $L_y = 1$. For all cases, the values for L_x, L_y, and L_z are constrained: they must each be positive and $L_x + L_y + L_z = 1$. To a reasonable approximation, they are also proportional to the inverse of the respective ellipsoid axis length. Since this formulation does not account for interactions between dipoles (or higher order multi-poles), its accuracy is limited to cases where the distribution of the ellipsoids is sparse. The Bruggeman approximation attempts to correct this limitation by replacing the host permittivity ε_0 in Eq. (1) with the effective medium permittivity ε_{eff}. This approximation also puts all of the constituent materials on an equal footing. For a two component composite material ($N = 2$), assuming that $\varepsilon_0 = \varepsilon_{\text{eff}}$, Eq. (1) can be solved for the effective permittivity,

$$\varepsilon_{\text{eff}} = \frac{\varepsilon_1(f_1 - L) + \varepsilon_2(f_2 - L) \pm \sqrt{\left[\varepsilon_1(f_1 - L) + \varepsilon_2(f_2 - L)\right]^2 - 4\varepsilon_1\varepsilon_2 L(L-1)}}{2(1-L)} \tag{2}$$

The sign is chosen to ensure that the result gives a physically sensible permittivity. The result for spheres ($L = 1/3$ for all directions) is the isotropic Bruggeman EMA (IBEMA) that is used extensively to model interfacial roughness in ellipsometry measurements of thin film stacks [23,25]. However, an anisotropic model might be better for modeling edge roughness since this type of roughness may have a preferred orientation. The Bruggeman effective medium approximation can be extended to anisotropic media by allowing different depolarization factors for two or more directions in Eq. (2). Implementations of anisotropic EMAs have been studied for modeling

structured thin films [28], but to our knowledge generalized anisotropic EMAs have not yet been used to study random perturbations to an otherwise one dimensionally periodic surface structure.

The case of $L_x = L_z = 0$ and $L_y = 1$ reduces to form birefringence, which is appropriate for modeling sub-wavelength lamellar gratings [29]. Because this form of EMA is common for modeling form birefringent diffractive optical elements, we will refer to this approximation as the form birefringence effective medium approximation (FBEMA). In this case, the permittivity reduces to

$$\varepsilon_x = \varepsilon_z = (1-f)\varepsilon_0 + f\varepsilon_1$$

and

$$\varepsilon_y = [(1-f)\varepsilon_0^{-1} + f\varepsilon_1^{-1}]^{-1}$$

The form birefringence model has been suggested for modeling line edge roughness in the past [30]. However, as applied to roughness, two important assumptions are made in deriving the expressions for form birefringence: (a) the characteristic length of the roughness is small compared with the wavelength of the incident light, and (b) the amplitude of the roughness is large compared with the characteristic length of the roughness. The latter assumption is not typically valid for LER. The latter assumption is not typically valid for LER, and the results shown later in this paper are never fully consistent with this model.

5. RESULTS

Figure 2 shows the angular dependence of the reflectance at a wavelength of 633 nm for the two polarizations for the nominal 200 nm pitch, 100 nm width, 200 nm height grating and the ensemble-averaged reflectances for the same gratings with self-affine random roughness (σ = 2.5 nm,

ξ = 20 nm, α = 0.5) calculated by 2DRCW. The cross-polarized reflectances are not shown, but were found to be less than 10^{-6}. The differences between the reflectances depend upon angle, and for this particular example, the effects are predominantly in the s-polarized reflectance.

As a measure of how much the reflectances change as various parameters change, the rms difference between the reflectances calculated with roughness and those calculated for the nominal grating was determined as a function of roughness parameters. Figure 5 shows the dependence of this rms difference on rms roughness, correlation length, and roughness exponent. As expected, the dependence upon rms roughness starts from zero, when the rough grating is identical to the nominal grating. There is also some dependence upon the roughness exponent and the correlation length, which suggests that a single EMA model is unlikely to be successful for all roughness conditions.

Figure 6 shows the difference between the reflectance from the grating with LER and reflectance from the nominal grating (shown in Figure 2), together with the differences calculated using 1DRCW simulations with EMA layers. We choose to show the limiting EMA cases described above, in particular, the isotropic Bruggeman EMA ($L_x = L_y = L_z = 1/3$), the anisotropic Bruggeman EMA ($L_x = L_y = 1/2$ and $L_z = 0$), and the form birefringence EMA ($L_x = L_z = 0$ and $L_y = 1$). An optimized case that is discussed later in the paper ($L_x = 0.7, L_y = 0.3$ and $L_z = 0$) is also shown for comparison. The thicknesses of the EMA layers in these calculations were set to $t = 2\sigma$. There is not perfect quantitative agreement between the EMA model and the 2DRCW simulation, yet there are qualitative similarities that suggest that the EMA model can provide a rough estimate of the effects one would expect to observe from roughness.

While the limiting cases for the EMA theories do not match the 2DRCW simulations well, we consider whether optimizing the values of L_x, L_y, and L_z would yield a significantly improved match between the models. After all, the roughness studied with the 2DRCW simulations is neither isotropic nor does it exhibit infinite or zero length scales. To optimize the values of L_x, L_y, and L_z, we calculate the metric

$$S_{s,p} = \sqrt{\frac{1}{N}\sum_{i=1}^{N}\left[R_{s,p}^{\text{EMA}}(\theta_i) - R_{s,p}^{\text{2DRCW}}(\theta_i)\right]^2} \tag{4}$$

where $R_{s,p}^{\text{EMA}}(\theta_i)$ is the reflectance calculated with 1DRCW and an EMA layer, $R_{s,p}^{\text{2DRCW}}(\theta_i)$ is the mean reflectance calculated using the 2DRCW with rough line edge profiles, θ_i is the *i*th incident angle, and N is the number of incident angles. Eq. (4) is simply the rms difference between the two theories. The subscript indicates the polarization.

Optimizing on a single polarization, however, does not yield an optimum solution for both polarizations. We thus chose the combined objective function

$$S = \sqrt{{S_s}^2 + {S_p}^2} \tag{5}$$

letting L_x, L_y, and L_z vary in 0.1 steps. We also varied the thickness t of the EMA region, but found that $t = 2\sigma$ yields the best results. Furthermore, we fixed the fill factor $f = 1/2$.

Figure 7 shows the optimal values of L_x, L_y, and L_z as a function of the correlation length ξ, holding the rms amplitude $\sigma = 2.5$ nm and the roughness exponent $\alpha = 0.5$ fixed. We find that the optimum values for L_z remained constant at 0, while the optimum values for L_x and L_y varied monotonically from approximately $L_x = 0.7$ and $L_y = 0.3$ at short correlation lengths to $L_x = 0.9$

and $L_y = 0.1$ at long correlation lengths. One can visualize ellipsoids of constant *z* and *x* axes whose *y* axis is short for short correlation lengths and long for long correlation lengths.

At this point, we have only discussed one measurement configuration (reflectance as a function of scanning incident angle) and one nominal grating. We also investigated a measurement where we held the incident angle fixed at $\theta = 65°$ and scanned the wavelength from 290 nm to 750 nm, using the nominal 200 nm pitch, 100 nm width, 200 nm height grating and roughness parameters σ = 2.5 nm, ξ = 20 nm, and α = 0.5. Figure 8 shows the resulting comparison between the 2DRCW simulations and the 1DRCW simulations with EMA layer parameters $L_x = 0.7, L_y = 0.3$ and $L_z = 0$. The agreement is reasonably good for s-polarization. The agreement is poorer for p-polarization, but there are still qualitative similarities. Wavelengths shorter than about 380 nm, where we have less confidence that the 2DRCW algorithm converged, yield progressively worse agreement.

We also considered varying the nominal grating. We held the pitch fixed (200 nm), but varied the height and width of the lines. Using the EMA model with parameters $L_x = 0.7, L_y = 0.3$ and $L_z = 0$, we report the rms model differences S_s and S_p. Figure 9 shows these results for both polarizations and five different nominal gratings. Changing the line width had little effect on the overall match between the models. Reducing the height improved the match significantly, but it should be borne in mind that scatterometry becomes less sensitive to other grating parameters as well for shallow gratings. For the tall lines, the match is substantially poorer.

6. CONCLUSIONS

EMA models can provide a computationally efficient method for modeling the effects of LER in scatterometry measurements. In this paper we discussed a comparison between signatures obtained

from EMA models for LER and those calculated with 2DRCW on rough line edge profiles. While the agreement was not always perfect, they were sufficiently good to estimate the overall magnitude of the effects of LER in a measurement. By further refining the EMA, we can improve the agreement between the simulations. We found that, for this particular case, using an anisotropic EMA with parameters $L_x = 0.7, L_y = 0.3$ and $L_z = 0$ yielded much better results for short correlation length LER than the other models that were considered.

7. ACKNOWLEDGMENTS

The authors would like to thank Heather Patrick and Gregg Gallatin for their valuable insights and useful comments on this work.

REFERENCES

1. K. Huang, B. J. Rice, B. Coombs, and R. Freed, “Methods For evaluating lithographic performance of exposure tools for the 45-nm node: ECD and scatterometry,” in *Metrology, Inspection, and Process Control for Microlithography XVIII*, R. M. Silver, Ed., Proc. SPIE **5375**, 494-502 (2004).

2. E. Barouch, and S. L. Knodle, “Scatterometry as a practical in-situ metrology technology,” in *Metrology, Inspection, and Process Control for Microlithography XVII,* D.J. Herr, Ed., Proc. SPIE **5038**, 559-567 (2003).

3. D. Herisson, D. Neira, C. Fernand, P. Thony, D. Henry, S. Kremer, M. Polli, M. Guevremont, and A. Elazami, “Spectroscopic ellipsometry for lithography front-end level CD control: a complete analysis for production integration,” in *Metrology, Inspection, and Process Control for Microlithography XVII,* D.J. Herr, Ed., Proc. SPIE **5038**, 264-273 (2003).

4. R. Silver, T. Germer, R. Attota, B.M. Barnes, B. Bunday, J. Allgair, E. Marx, and J. Jun, "Fundamental limits of optical critical dimension metrology: a simulation study," in *Metrology, Inspection, and Process Control for Microlithography XXI*, C. N. Archie, Ed., Proc. SPIE **6518**, 65180U (2007).

5. T. A. Germer, "Effect of line and trench profile variation on specular and diffuse reflectance from a periodic structure," J. Opt. Soc. Am. A **24**, 696-701 (2007).

6. P. Boher, J. Petit, T. Leroux, J. Foucher, Y. Desieres, J. Hazart, and P. Chaton, "Optical Fourier transform scatterometry for LER and LWR metrology," in Metrology, Inspection, and Process Control for Microlithography XIX, R.M. Silver, Ed. Proc. SPIE **5752**, 192–203 (2005).

7. B. Yaakobovitz, Y. Cohen, and Y. Tsur, "Line edge roughness detection using deep UV light scatterometry," Microelectronic Eng. **84**, 619–625 (2007).

8. T. Schuster, S. Rafler, V. F. Paz, K. Frenner, and W. Osten, "Fieldstitching with Kirchhoff-boundaries as a model based description for line edge roughness (LER) in scatterometry," Microelectronic Eng. **86**, 1029–1032 (2009).

9. L. F. Li, "New formulation of the Fourier modal method for crossed surface-relief gratings," J. Opt. Soc. Am. A **14**, 2758-2767 (1997).

10. M. G. Moharam, E. B. Grann, D. A. Pommet, and T. K. Gaylord, "Formulation for stable and efficient implementation of the rigorous coupled-wave analysis of binary gratings," J. Opt. Soc. Am. A **12**, 1068-1076 (1995).

11. M. G. Moharam, D. A. Pommet, E. B. Grann, and T. K. Gaylord, "Stable implementation of the rigorous coupled-wave analysis for surface-relief gratings–enhanced transmittance matrix approach," J. Opt. Soc. Am. A **12**, 1077–1086 (1995).

12. L. F. Li, “Use of Fourier series in the analysis of discontinuous periodic structures,” J. Opt. Soc. Am. A **13**, 1870-1876 (1996).

13. P. Lalanne and G. M. Morris, “Highly improved convergence of the coupled-wave method for TM polarization,” J. Opt. Soc. Am. A **13**, 779-784 (1996).

14. K. A. Michalski and T. A. Germer, unpublished.

15. T. A. Germer, "SCATMECH: Polarized Light Scattering C++ Class Library," available online at http://physics.nist.gov/scatmech (2008).

16. G. M. Gallatin, “Resist blur and line edge roughness,” in *Optical Microlithography XVIII*, B.W. Smith, Ed., Proc. **5754**, 38–52 (2005).

17. V. Constantoudis, G. P. Patsis, L. H. A. Leunissen, and E. Gogolides, “Toward a complete description of linewidth roughness: a comparison of different methods for vertical and spatial LER and LWR analysis and CD variation,” in *Metrology, Inspection, And Process Control For Microlithography XVIII*, R.M. Silver, Ed., Proc. SPIE **5375**, 967– 977 (2004).

18. V. Constantoudis, G. Kokkoris, P. Xydi, E. Gogolides, E. Pargon, And M. Martin, “Line edge roughness transfer during plasma etching: modeling approaches and comparison with experimental results,” in *Advances in Resist Materials and Processing Technology XXVI*, C.L. Henderson, Ed., Proc. SPIE **7273**, 72732J (2009).

19. V. Constantoudis, G.P. Patsis, and E. Gogolides, “Photoresist line-edge roughness analysis using scaling concepts,” J. of Microlithography, Microfabrication, and Microsystems **3**, 429 (2004).

20. V. Constantoudis, G.P. Patsis, A. Tserepi, and E. Gogolides, “Quantification of line-edge roughness of photoresists II: scaling and fractal analysis and the best roughness descriptors," J. Vac. Sci. & Technol. B **21**, 1019 (2003).

21. G.P. Patsis, V. Constantoudis, A. Tserepi, E. Gogolides, and G. Grozev, “Quantification of line-edge roughness of photoresists. I. a comparison between off-line and on-line analysis of top-down scanning electron microscopy images,” J. Vac. Sci. & Technol. B **21**, 1008 (2003).

22. J. Thiault, J. Foucher, J.H. Tortai, O. Joubert, S. Landis, and S. Pauliac, “Line edge roughness characterization with a three-dimensional atomic force microscope: transfer during gate patterning processes,” J.Vac. Sci. & Technol. B **23**, 3075 (2005).

23. D.E. Aspnes, J.B. Theeten, and F. Hottier, “Investigation of effective-medium models of microscopic surface roughness by spectroscopic ellipsometry,” Phys. Rev. **B 20**, 3292–3302 (1979).

24. D. Ronnow, S.K. Anderson, and G.A. Niklasson, “Surface roughness effects in ellipsometry: comparison of truncated sphere and effective medium models," Opt. Mat. **4**, 815–821 (1995).

25. H.G. Tompkins, *A User’s Guide to Ellipsometry* (Academic Press, San Diego,1993).

26. J.C. Maxwell Garnett, “Colours in metal glasses, in metallic films, and in metallic solutions–II,” Proc. of the Royal Society of London. Series A **205**, 237–288 (1906).

27. L. Rayleigh, “On the incidence of aerial and electric waves upon small obstacles in the form of ellipsoids or elliptic cylinders, and on the passage of electric waves through a circular aperture in a conducting screen,” Philosophical Magazine **44**, 28–52 (1897).

28. T. G. Makay, “Homogenization of linear and nonlinear complex composite materials,” in *Introduction to complex mediums for optics and electromagnetic*, W.S. Weiglhofer, A. Lakhtakia, Eds., pp. 317–346 (SPIE, Bellingham, Washington, 2003).

29. M. Born, and E. Wolf, *Principles of Optics,* Sixth Edition (Pergamon Press, Oxford, 1980) pp. 705–708.

30. J. Bischoff, E. Drege, and S. Yedur, “Edge Roughness Measurement In Optical Metrology,” US Patent #7,046,375.

FIGURE CAPTIONS

Figure 1 Schematic representations of the structures used in the simulations. The figures show (a) the nominal profile, (b) a 2D periodic profile used to directly calculate the effect of LER using a 2D RCW algorithm, and (c) a 1D periodic profile used to approximate the effect of the LER with an effective medium layer. The magnitudes of the roughness are exaggerated and the figure is not to scale.

Figure 2 Reflectance from a silicon grating with P_x = 200 nm, w = 100 nm, and h = 200 nm simulated for wavelength λ = 632.8 nm. The curves represent (solid line) s-polarization and (dashed line) p-polarization for the nominal grating. The symbols represent (■) s-polarization and (□) p-polarization for a grating with LER defined by a self-affine function with σ = 2.5 nm, ξ = 20 nm, and α = 0.5.

Figure 3 Examples of line edge profiles used in the simulations: (a) self-affine profile with ξ = 20 nm and α = 0.5, (b) self-affine profile with ξ = 20 nm and α = 1.0, (c) self-affine profile with ξ = 100 nm and α = 0.5, (d) self-affine profile with ξ = 20 nm and α = 0.75, (e) sinusoidal profile with P_y = 20 nm, and (f) rectangular profile with P_y = 20 nm. The rms roughness values are 5 nm and the sides of the square boxes are 200 nm.

Figure 4 The change in reflectance between the nominal grating with P_x = 200 nm, w = 100 nm, and h = 200 nm and (solid curve) that with random LER defined by ξ = 20 nm and α = 0.5, (dashed

curve) that with a rectangular roughness profile with P_y = 20 nm, and (dotted curve) that with a sinusoidal roughness profile having P_y = 20 nm. The rms roughness was 2.5 nm for all three curves.

Figure 5 The rms change in reflectance calculated by 2DRCW as a function of rms amplitude σ, correlation length ξ, and roughness exponent α as described in the text. For each graph the roughness parameters that are not varied are fixed at $\alpha = 0.5$, $\xi = 20$ nm, and $\sigma = 2.5$ nm. The data are for (■) s-polarization and (□) p-polarization.

Figure 6 The change in reflectance between the nominal grating and (solid squares) the grating with LWR defined by $\sigma = 2.5$ nm, $\xi = 20$ nm, $\alpha = 0.5$ calculated using a 2DRCW algorithm; (solid line) the reflectance calculated using a 1DRCW algorithm and an EMA with $(L_x, L_y, L_z) = (0,1,0)$; (dotted line) the reflectance calculated using a 1DRCW algorithm and an EMA with $(L_x, L_y, L_z) = (0.5,0.5,0)$; (long-dashed line) the reflectance calculated using a 1DRCW algorithm and an EMA with $(L_x, L_y, L_z) = (1/3,1/3,1/3)$; and (short-dashed line) the reflectance calculated using a 1DRCW algorithm and an EMA with $(L_x, L_y, L_z) = (0.7,0.3,0)$. The nominal grating has P_x = 200 nm, w = 100 nm, and h = 200 nm. The fill factor was $f = 0.50$ and the thickness of the effective medium layer was $t = 2\sigma$ in all cases.

Figure 7 Best fit EMA parameters (■) L_x, (□) L_y, and (Δ) L_z as functions of roughness correlation length.

Figure 8 Wavelength dependent specular reflectance differences for an incident angle of 65° for (solid lines) the nominal grating with P_x = 200 nm, w = 100 nm, and h = 200 nm, (solid lines) for

the grating with LER defined by $\sigma = 2.5$ nm, $\xi = 20$ nm, $\alpha = 0.5$ calculated using a 2DRCW algorithm, and (dots) for the grating with an effective medium layer defined by $(L_x, L_y, L_z) = (0.7, 0.3, 0)$, $f = 50$ %, and $t = 2\sigma$.

Figure 9 Objective functions (S_s and S_p) for various gratings with LER defined by $\sigma = 2.5$ nm, $\xi = 20$ nm, $\alpha = 0.5$. All the gratings have $P_x = 200$ nm.

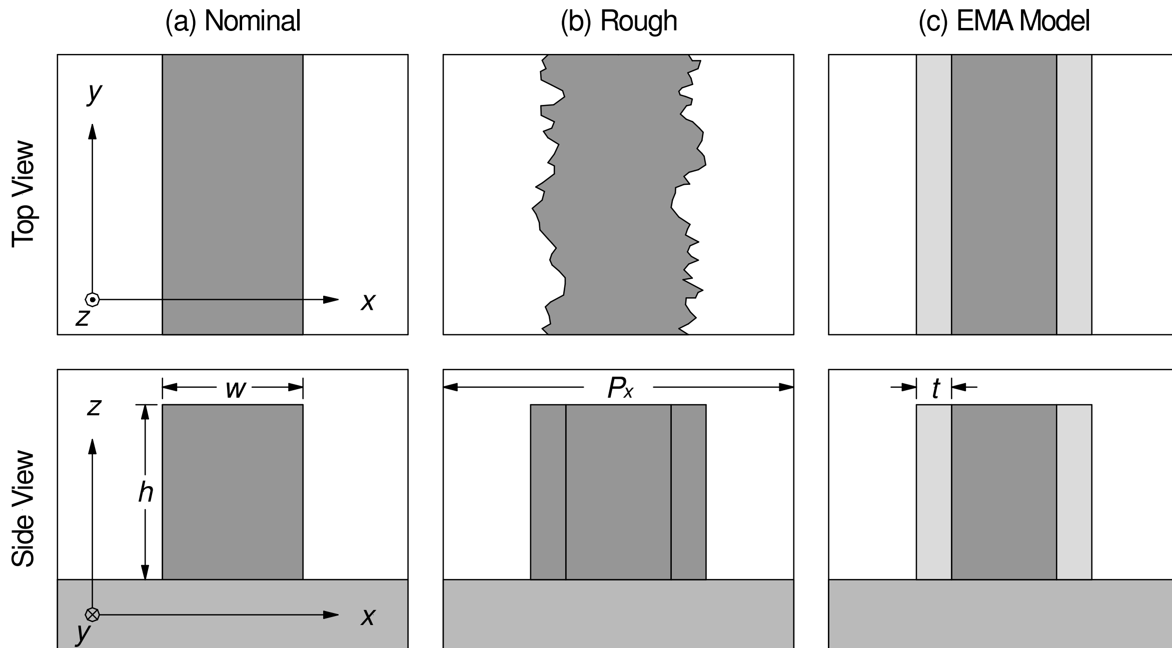

Figure 1 Schematic representations of the structures used in the simulations. The figures show (a) the nominal profile, (b) a 2D periodic profile used to directly calculate the effect of LER using a 2D RCW algorithm, and (c) a 1D periodic profile used to approximate the effect of the LER with an effective medium layer. The magnitudes of the roughness are exaggerated and the figure is not to scale.

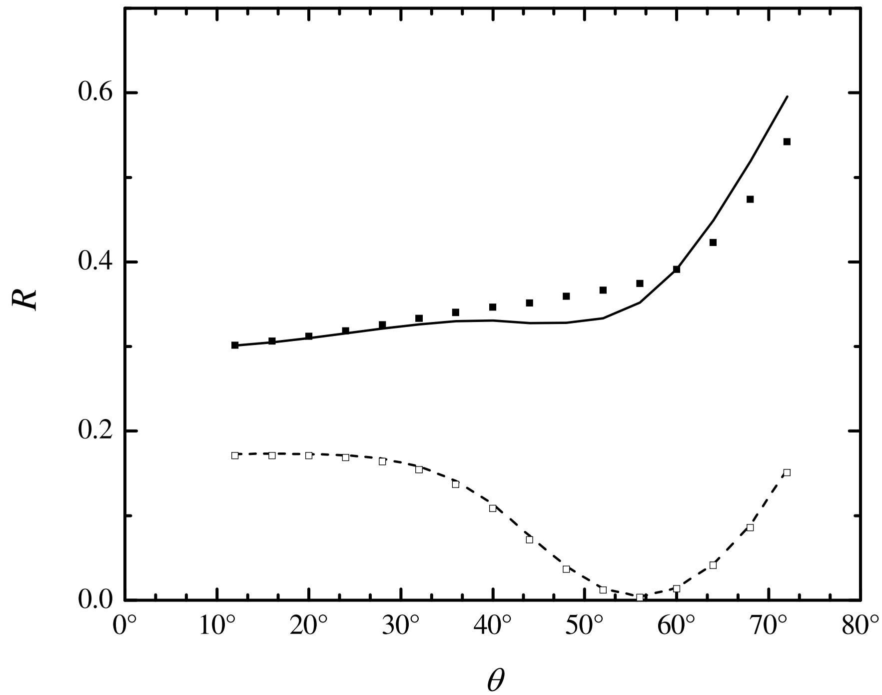

Figure 2 Reflectance from a silicon grating with P_x = 200 nm, w = 100 nm, and h = 200 nm simulated for wavelength λ = 632.8 nm. The curves represent (solid line) s-polarization and (dashed line) p-polarization for the nominal grating. The symbols represent (■) s-polarization and (□) p-polarization for a grating with LER defined by a self-affine function with σ = 2.5 nm, ξ = 20 nm, and α = 0.5.

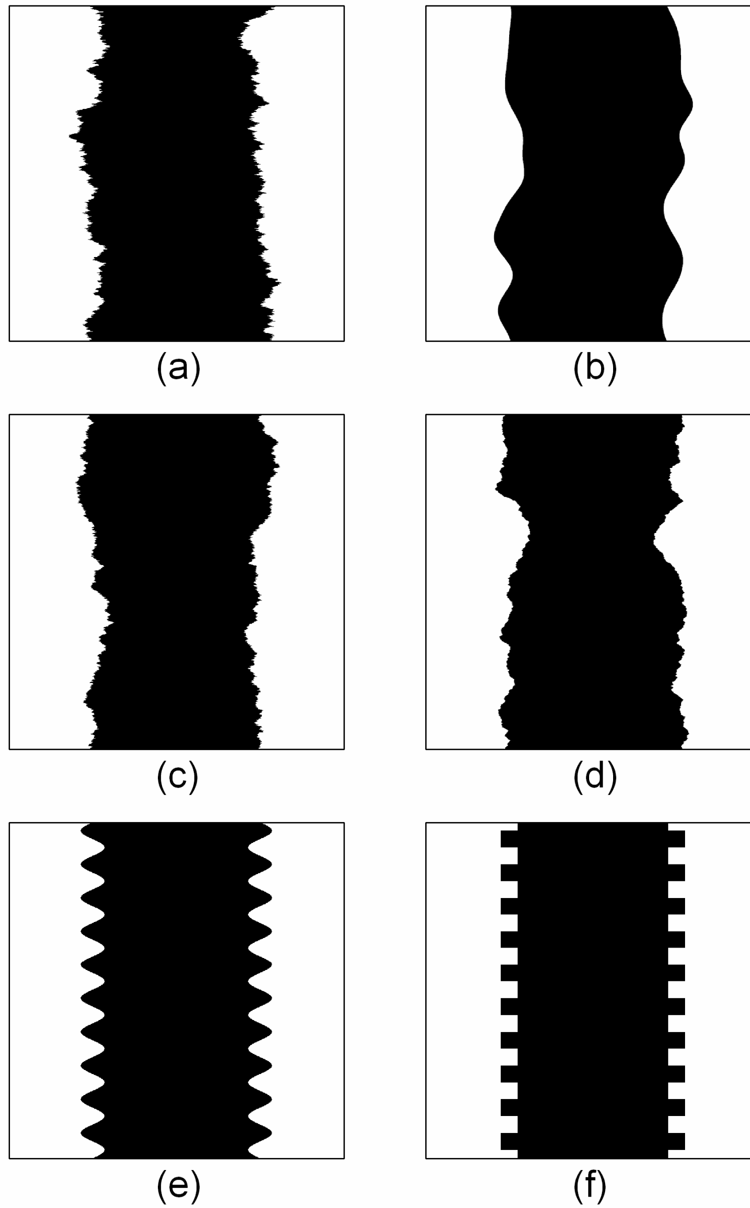

Figure 3 Examples of line edge profiles used in the simulations: (a) self-affine profile with $\xi = 20$ nm and $\alpha = 0.5$, (b) self-affine profile with $\xi = 20$ nm and $\alpha = 1.0$, (c) self-affine profile with $\xi = 100$ nm and $\alpha = 0.5$, (d) self-affine profile with $\xi = 20$ nm and $\alpha = 0.75$, (e) sinusoidal profile with $P_y = 20$ nm, and (f) rectangular profile with $P_y = 20$ nm. The rms roughness values are 5 nm and the sides of the square boxes are 200 nm.

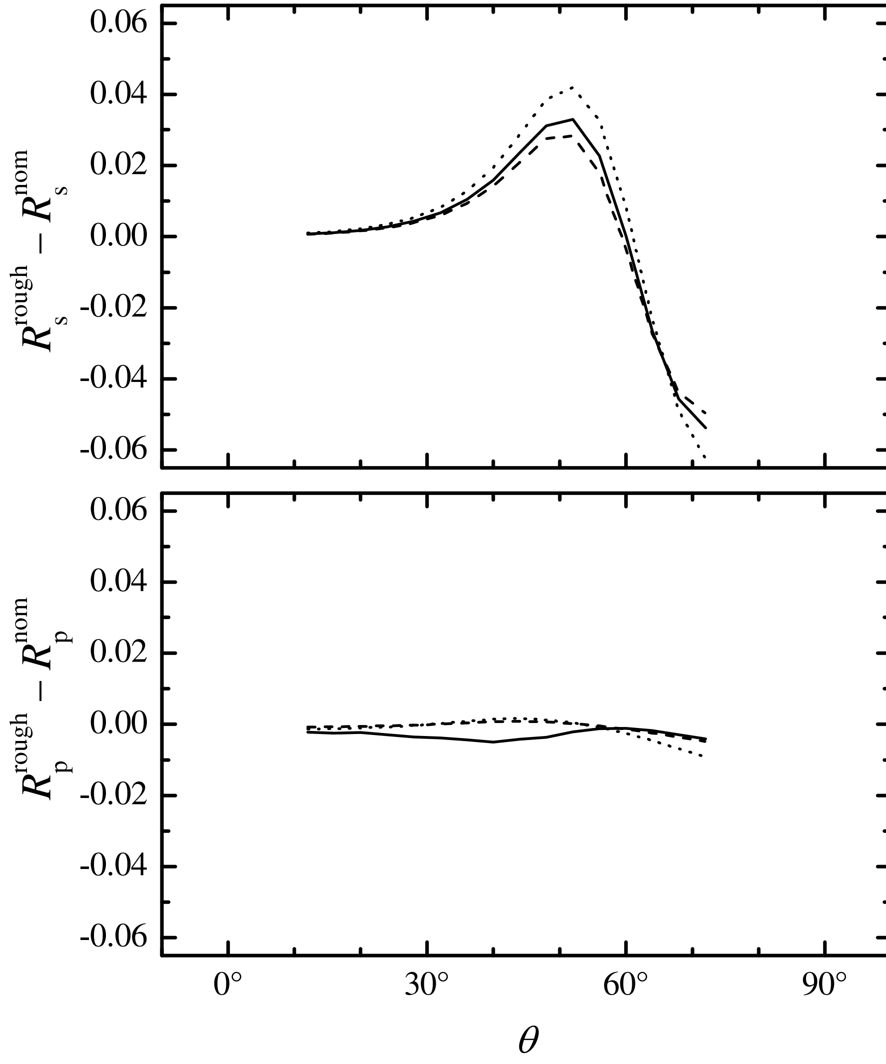

Figure 4 The change in reflectance between the nominal grating with P_x = 200 nm, w = 100 nm, and h = 200 nm and (solid curve) that with random LER defined by ξ = 20 nm and α = 0.5, (dashed curve) that with a rectangular roughness profile with P_y = 20 nm, and (dotted curve) that with a sinusoidal roughness profile having P_y = 20 nm. The rms roughness was 2.5 nm for all three curves.

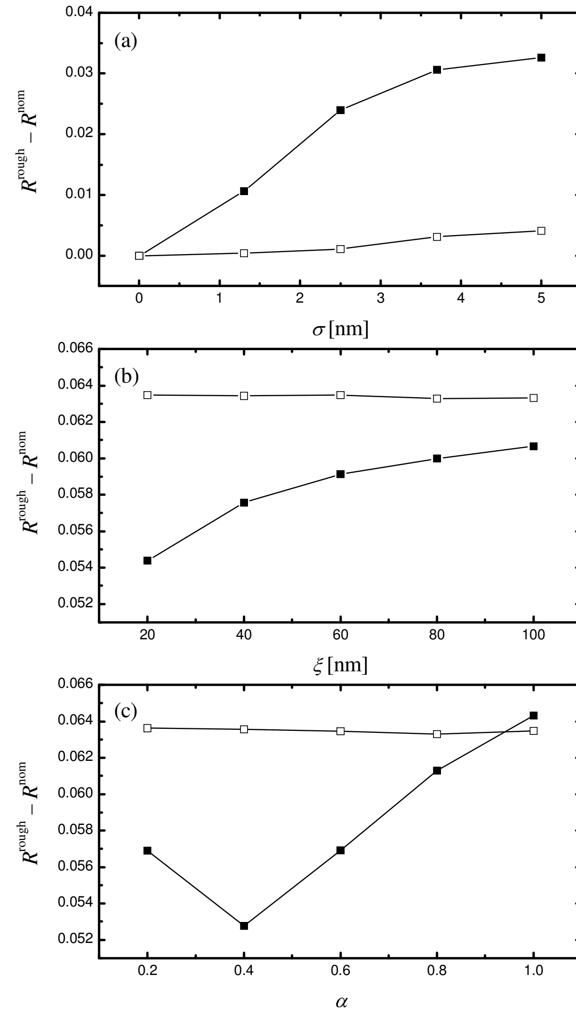

Figure 5 The rms change in reflectance calculated by 2DRCW as a function of rms amplitude σ, correlation length ξ, and roughness exponent α as described in the text. For each graph the roughness parameters that are not varied are fixed at $\alpha = 0.5$, $\xi = 20$ nm, and $\sigma = 2.5$ nm. The data are for (■) s-polarization and (□) p-polarization.

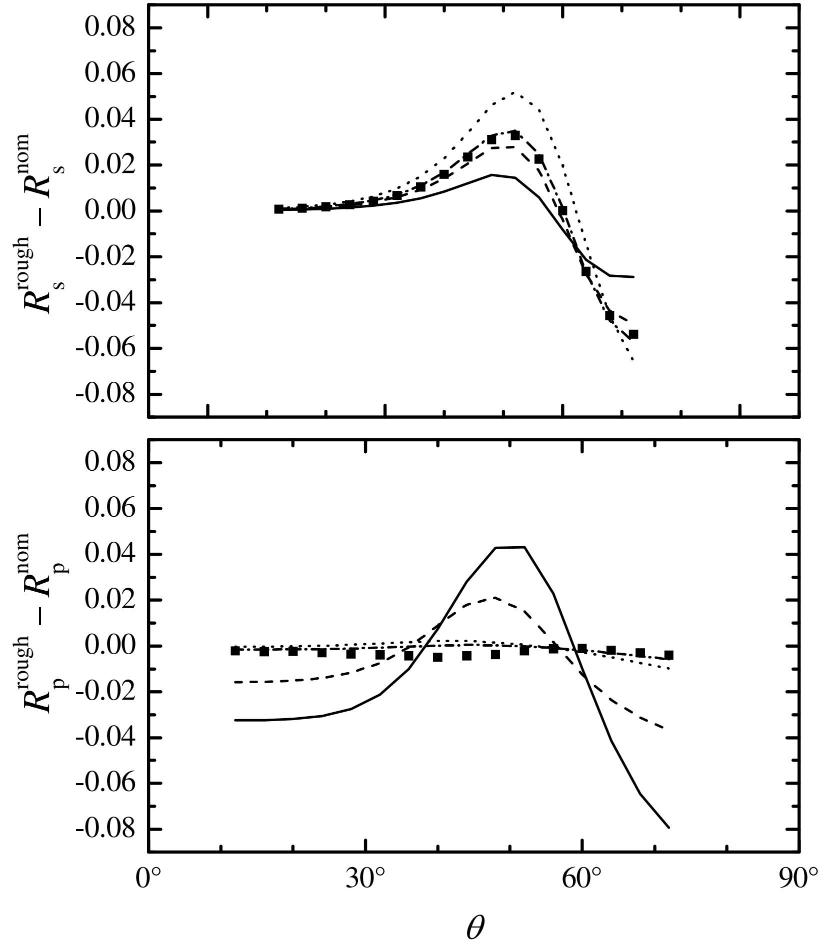

Figure 6 The change in reflectance between the nominal grating and (solid squares) the grating with LWR defined by σ = 2.5 nm, ξ = 20 nm, α = 0.5 calculated using a 2DRCW algorithm; (solid line) the reflectance calculated using a 1DRCW algorithm and an EMA with (L_x, L_y, L_z) = (0,1,0); (dotted line) the reflectance calculated using a 1DRCW algorithm and an EMA with (L_x, L_y, L_z) = (0.5,0.5,0); (long-dashed line) the reflectance calculated using a 1DRCW algorithm and an EMA with (L_x, L_y, L_z) = (1/3,1/3,1/3); and (short-dashed line) the reflectance calculated using a 1DRCW algorithm and an EMA with (L_x, L_y, L_z) = (0.7,0.3,0). The nominal grating has P_x = 200 nm, w = 100 nm, and h = 200 nm. The fill factor was f = 0.50 and the thickness of the effective medium layer was $t = 2\sigma$ in all cases.

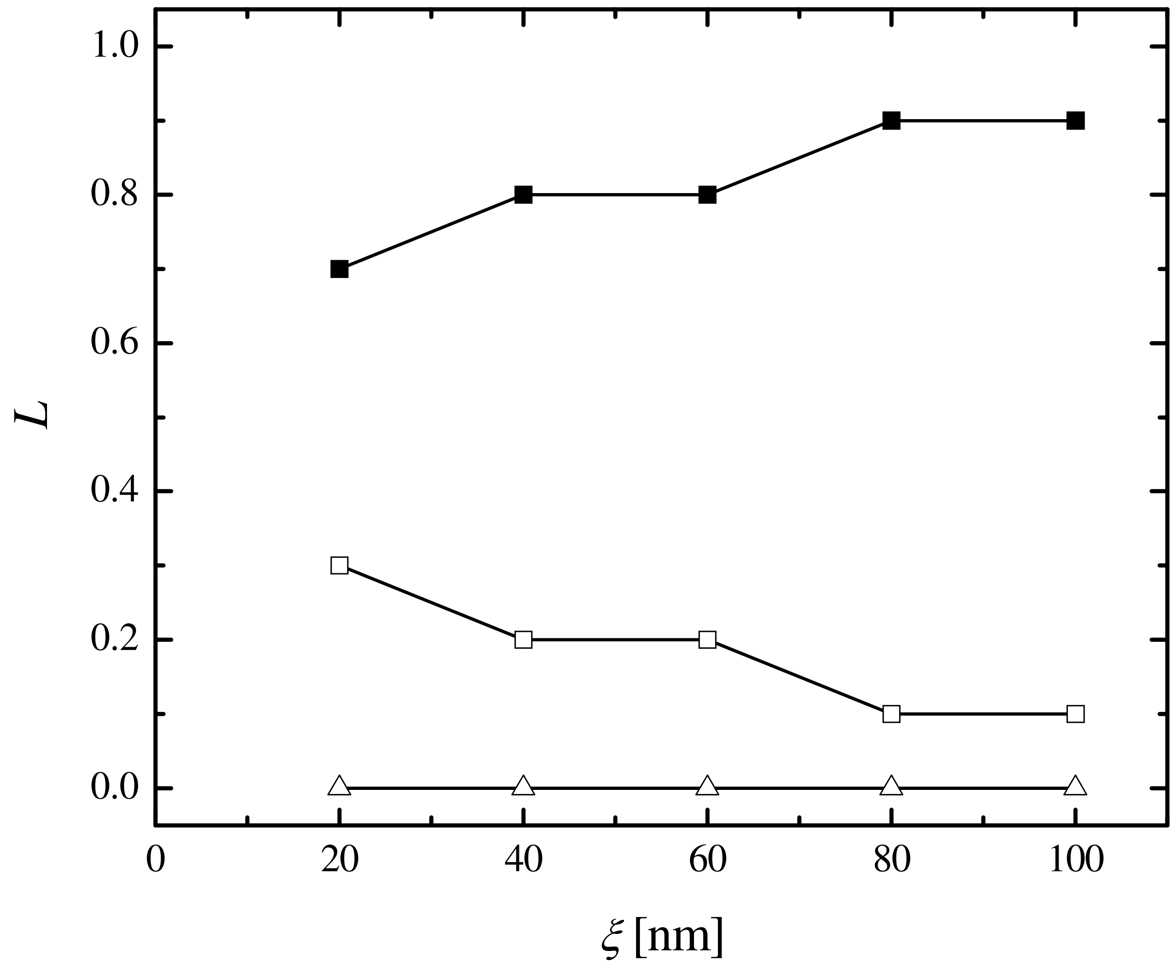

Figure 7 Best fit EMA parameters (■) L_x, (□) L_y, and (Δ) L_z as functions of roughness correlation length.

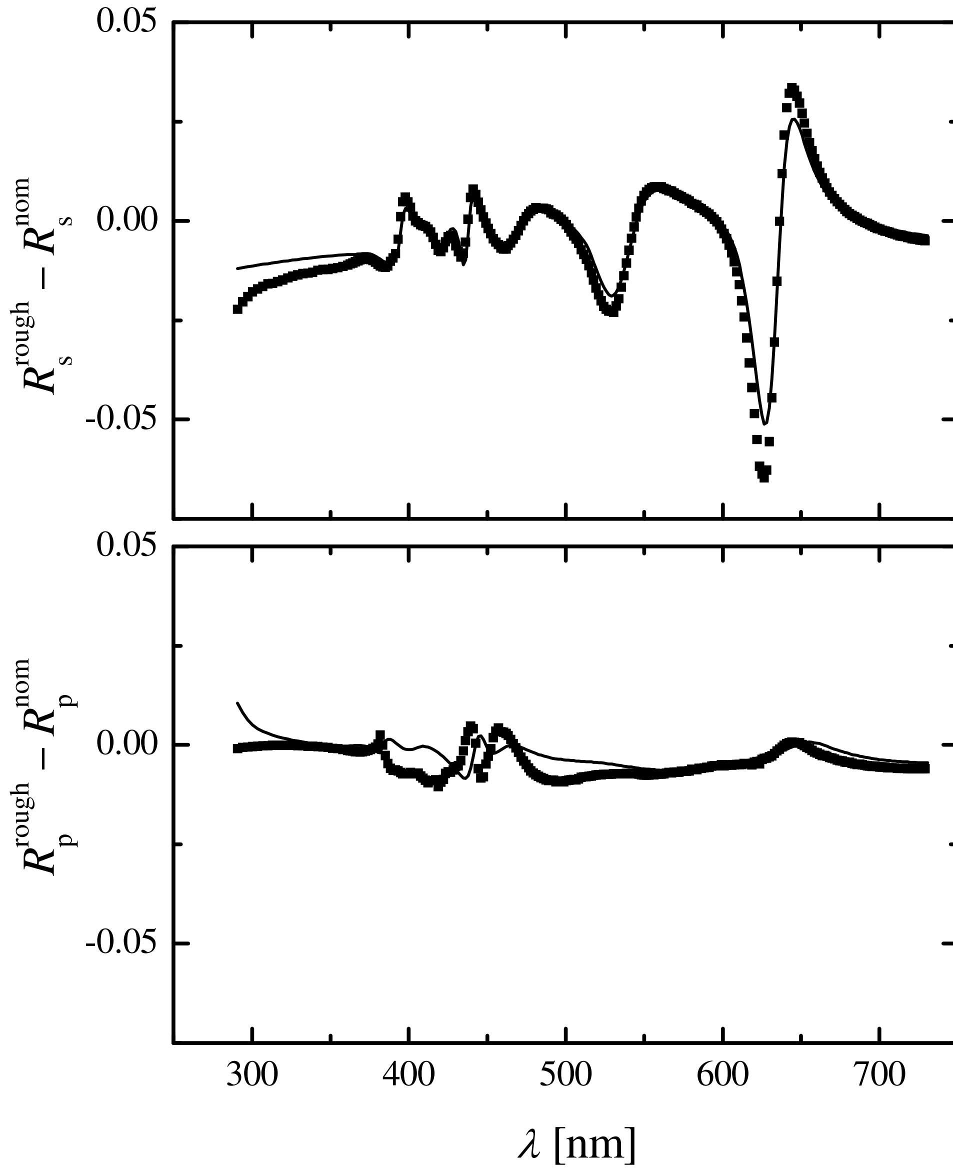

Figure 8 Wavelength dependent specular reflectance differences for an incident angle of 65° for (solid lines) the nominal grating with P_x = 200 nm, w = 100 nm, and h = 200 nm, (solid lines) for the grating with LER defined by σ = 2.5 nm, ξ = 20 nm, α = 0.5 calculated using a 2DRCW algorithm, and (dots) for the grating with an effective medium layer defined by (L_x, L_y, L_z) = (0.7, 0.3, 0), f = 50 %, and t = 2σ.

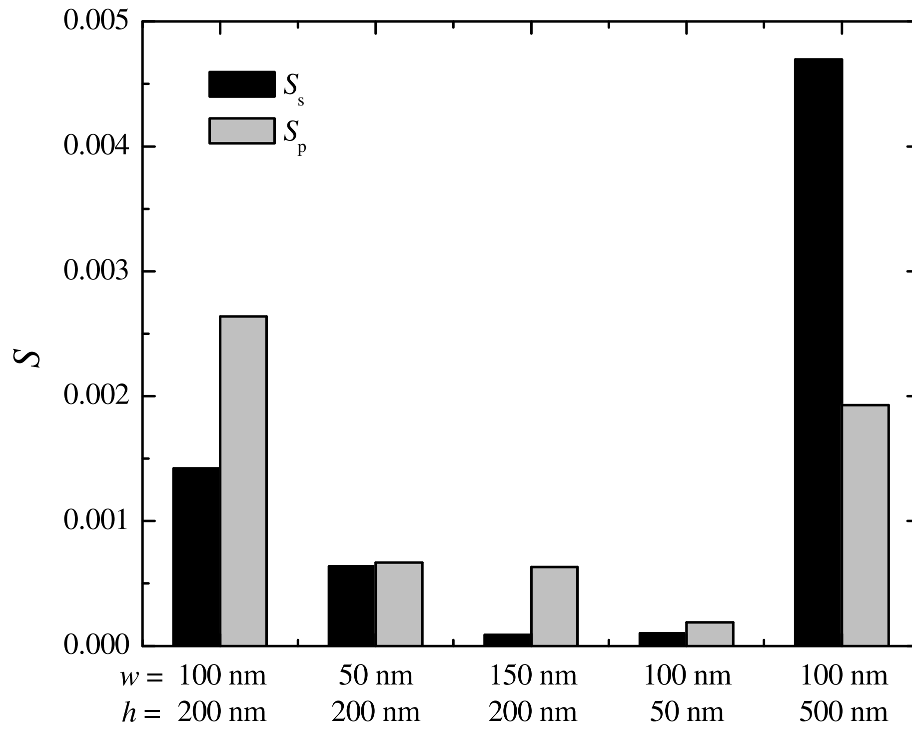

Figure 9 Objective functions (S_s and S_p) for various gratings with LER defined by $\sigma = 2.5$ nm, $\xi = 20$ nm, $\alpha = 0.5$. All the gratings have $P_x = 200$ nm.